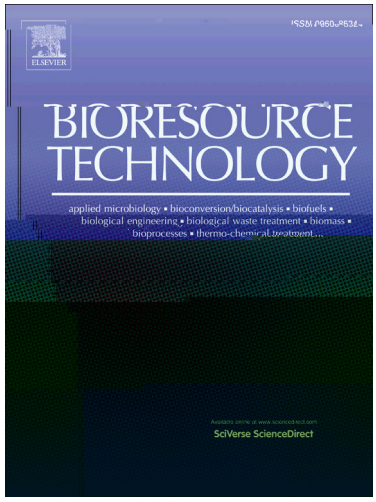

Comparative evaluation of thermal oxidative decomposition for oil–plant residues via thermogravimetric analysis: Thermal conversion characteristics, kinetics, and thermodynamics

Jianbiao Chen, Yanhong Wang, Xuemei Lang, Xiu'e Ren, Shuanshi Fan

PII: S0960-8524(17)30920-3
DOI: http://dx.doi.org/10.1016/j.biortech.2017.06.033
Reference: BITE 18270

To appear in: *Bioresource Technology*

Received Date: 19 April 2017
Revised Date: 5 June 2017
Accepted Date: 6 June 2017

Please cite this article as: Chen, J., Wang, Y., Lang, X., Ren, X., Fan, S., Comparative evaluation of thermal oxidative decomposition for oil–plant residues via thermogravimetric analysis: Thermal conversion characteristics, kinetics, and thermodynamics, *Bioresource Technology* (2017), doi: http://dx.doi.org/10.1016/j.biortech.2017.06.033

1. Introduction

With increasing awareness of the whole world on energy security, ecological environment, and global climate change, quickening the development and utilization of renewable energy has been the general consensus and concerted action by all countries (Zhou et al., 2011; Omer, 2008; Hassan et al., 2016). As pointed out by the UN's Intergovernmental Panel on Climate Change (IPCC), International Energy Agency (IEA), and International Renewable Energy Agency (IREA), the promotion of renewable energy sources like solar, tide, geothermal, and biomass will be one of the vital measures to control climate change (Ogle et al., 2014; Bhattacharya et al., 2016; Kravanja et al., 2015). To establish a clean and low–carbon energy system, the Chinese Government has set a goal to increase the share of non–fossil energy in total primary energy consumption to 15% by 2020, and to 20% by 2030 (Chen et al., 2015a). Among various renewables, biomass is deemed as the only carbon–based alternative energy, which can be transformed into a series of high value–added biofuels or intermediate compounds for energy and chemical industry (Werther et al., 2000; Yahya et al., 2015). Although CO_2 emissions are inevitable during the consumption of biomass, the same amount of CO_2 was fixed from the atmosphere through photosynthesis in the process of their growth. The potential of CO_2 neutral will be gained by using biomass as fuels. Furthermore, it was also proved that utilizing biomass as an alternative fuel would release less SO_2, NO_x, particulate matters, and other gaseous pollutants (Wu et al., 2014; Gai et al., 2015). Therefore, promoting biomass can not only reduce the reliance on fossil fuels, but also reduce the atmospheric pollution and CO_2 greenhouse effect.

In theory, all biomass resources can be treated as feedstocks to mitigate the shortage of fossil fuels and environmental pollution. However, there is some controversy when biomass resources

CS, and CM) in air atmosphere. The thermal analysis experiments were performed in a thermogravimetric analyzer (TGA) at four different heating rates. On basis of Coats–Redfern approach, the kinetic triplets of the thermal oxidative decomposition of RS, RM, CS, and CM were carefully determined. The existence of kinetic compensation effect at different heating rates was also analyzed. Finally, the thermodynamic parameters, i.e. the changes of enthalpy (ΔH), Gibbs free energy (ΔG), and entropy (ΔS), of individual conversion zone of RS, RM, CS, and CM at peak temperature were calculated by the activated complex theory.

2. Materials and methods

2.1. Raw materials and characterization

As two common oil–bearing crops cultivated in southern China, rape and camellia have four typical processing residues (RS, RM, CS, and CM), which were selected as the feedstocks for combustion. Before the thermal oxidative tests, these raw materials were carefully milled and sieved to get uniform particle with a range of 180–350 μm. After above treatments, the samples were placed in a desiccator for subsequent evaluations.

To characterize the basic properties of raw materials, the proximate analysis and ultimate analysis were carried out by the Laboratory Analytical Procedures (LAP) proposed by National Renewable Energy Laboratory (NREL). As shown in Table 1, all oil–plant residues have a high content of volatile matter (VM) and low content of fixed carbon (FC) and ash (A). It can be seen that the contents of VM and A of RS (CS) were higher than those of corresponding meal (RM, CM), but the content of FC of RS (CS) were lower. As for the ultimate analysis, the contents of C, H, N, and S in RS (CS) were relatively lower than those in RM (CM). Beyond that, the main chemical functional groups on the surface of four oil–plant residues were detected by the Nicolet

6700 Flex Fourier–transform infrared (FTIR) spectrometer (Thermo Fisher Scientific, USA). The FTIR spectra of oil–plant residues were gained by the potassium bromide (KBr) method with 0.09 cm^{-1} resolution and 4000–400 cm^{-1} wavelength.

2.2. Experimental apparatus and procedures

Thermal oxidative decomposition experiments of RS, RM, CS, and CM were performed on a STA 449C simultaneous thermogravimetric analyzer (NETZSCH, Germany). For minimizing the heat and mass transfer influences, the initial weight of oil–plant residues was maintained at a very small value of 8±0.2 mg. The biomass materials placed into the crucible of TGA were heated up from indoor temperature to 1273 K at the heating rates of 5, 10, 20, and 40 K min^{-1}. The oxidative atmosphere was supplied by the carrier gas of dry air. The air flow rate was kept at 80 mL min^{-1}, which was high enough to effectively eliminate secondary gas-fuels reactions. For each test, the control experiment was conducted for TG baseline correction without sample in the crucible. All the thermal oxidative decomposition exphmenies weo

Moreover, some combustion indices were also recommended to reflect the ignition, burnout, and comprehensive combustion performances of oil–plant residues under disparate conditions. These indices are the volatile matter release index (D_v) (Liu et al., 2013), ignition index (C_i) (Li et al., 2011), burnout index (C_b) (Li et al., 2011), and comprehensive combustibility index (S) (Liu et al., 2013). They can be described as the functions of characteristic temperatures and weight loss rates (Chen et al., 2015b).

$$D_v = \frac{-R_p}{T_v \times T_p \times \Delta T_{1/2}} \quad (1)$$

$$C_i = \frac{-R_p}{t_i \times t_p} \quad (2)$$

$$C_b = \frac{-R_p}{\Delta t_{1/2} \times t_p \times t_b} \quad (3)$$

$$S = \frac{(-R_p) \times (-R_v)}{T_i^2 \times T_b} \quad (4)$$

where t_i, t_p, t_b, and $\Delta t_{1/2}$ represent the ignition time, peak time, burnout time, and time interval at the half value of $-R_p$, respectively. T_v represents the initial devolatilization temperature. The detailed definitions for T_i, T_p, T_b, $-R_p$, $-R_v$, and $\Delta T_{1/2}$ are same as above.

3. Results and discussion

3.1. FTIR analysis of raw materials

The surface chemical structure of raw oil–plant residues (RS, RM, CS, and CM) was further investigated by FTIR technology. On basis of literature, the characteristic functional groups in the FTIR spectra can be divided into several regions (Gai et al., 2015; Li et al., 2015a, b): (1) 3700–3000 cm^{-1}, O–H stretching vibration for moisture and carbohydrate; (2) 2975–2845 cm^{-1}, C–H stretching vibration for methyl and methylene; (3) 1750–1680 cm^{-1}, C=O stretching

A

were identical, meaning that the contribution of heat from two stages was same. For other three samples, the heat released from the combustion was highly depended on chars oxidizing.

The thermal oxidative degradation characteristic parameters of RS, RM, CS, and CM in air at 10 K min^{-1} were listed in Table 2. For convenience, the thermal events during the combustion were subdivided into five zones on basis of above analysis, and took no account of the moisture release zone. Overall, the characteristic combustion temperatures (T_i, T_{p3}, T_{p5}, and T_b) of RS were lower than those of RM. Similarly, the characteristic temperatures of CS were lower than those of CM. With respect to the characteristic combustion rates ($-R_{p3}$, $-R_{p5}$, and $-R_v$), the values for RS (CS) were greater than those for RM (CM). Since RS and CS had lower combustion temperatures and higher combustion rates, the devolatilization, ignition, burnout, and comprehensive combustion performance were no doubt better than corresponding oil–plant meal.

3.2.2. Effect of heating rate

The effect of heating rate (β) on the thermal oxidative decomposition process of RS, RM, CS, and CM in air was investigated with four disparate heating rates of 5, 10, 20, and 40 °C min^{-1}. As depicted in Fig. 2, increasing β only moved TG curves of various oil–plant residues to a higher temperature region, without affecting the pattern of the thermal oxidative decomposition. These temperature shifts were the thermal hysteresis. It was due to better heat transfer effect would be gained at lower β. The similar findings have also been reported in the combustion of low–lipid microalgae (Gai et al., 2015), *Tetraselmis suecica* (Tahmasebi et al., 2013), fermentation residue (Du et al., 2013), *Chlorella vulgaris* (Chen et al., 2011), rice straw (Xie and Ma, 2013), and oil–palm biomass (Idris et al., 2012) at different β values. As shown in Fig. 3, with β increasing, the DTG curves extended to higher temperatures, and their values increased evidently.

w_i, w, and w_f are the initial weight, weight at time t, and final weight of each zone, respectively. A, E, R, and T represent the apparent pre–exponential factor $A=k_0 \cdot h(O_2)$, apparent activation energy, universal gas constant, and absolute temperature, respectively. For non–isothermal experiments conducting at constant heating rate $\beta=dT/dt$, the decomposition rate equation can be simplified and rearranged to the right part of Eq. (5).

The integral form of Eq. (5) can be written as follows (Vlaev et al., 2008):

$$g(x)=\int_0^x \frac{dx}{f(x)}=\frac{A}{\beta}\int_{T_0}^{T}\exp(-\frac{E}{RT})dT \tag{6}$$

where $g(x)$ is the integral form of reaction model.

The integral Coats–Redfern equation was used to approximately estimate the kinetic data of the thermal oxidative decomposition process of four oil–plant residues. Eq. (6) can be rewritten (Du et al., 2014; Chen et al., 2015b)

$$\ln\left[\frac{g(x)}{T^2}\right]=\ln\left[\frac{AR}{\beta E}\left(1-\frac{2RT}{E}\right)\right]-\frac{E}{RT} \tag{7}$$

The value of $2RT/E$ for the thermal oxidative decomposition of oil–plant residues was very close to zero, thus $1-2RT/E\approx 1$. Eq. (7) can be approximated as:

$$\ln\left[\frac{g(x)}{T^2}\right]=\ln\left[\frac{AR}{\beta E}\right]-\frac{E}{RT} \tag{8}$$

Based on Eq. (8), once the most appropriate kinetic model in Supplementary data (Vlaev et al., 2008) was selected, the regression line of $\ln[g(x)/T^2]$ against $1/T$ gave the highest correlation coefficient (R^2). The values of E and A were then determined.

Prior to thermal oxidative decomposition kinetics analysis, the conversion degrees x of the individual zone of RS, RM, CS, and CM were recalculated as a function of reaction temperature. The values of x utilized for kinetics analysis were in the range of 0.05–0.95. Taking the thermal

data obtained at 10 K min^{-1} as the examples, the regression lines of $\ln[g(x)/T^2]$ against $1/T$ for various thermal oxidative degradation zones of RS, RM, CS, and CM were drawn. As illustrated in Table 4, the highest R^2 values for various zones were in the range of 0.9873–0.9991, suggesting that the kinetic models selected were very suitable. The best kinetic models for various thermal oxidative decomposition stages of RS and CS were same, in order, $(1–x)^{3/2}$, $(1–x)^2$, $(1–x)^2$. The E values of the first and third stages from the thermal oxidative decomposition of RS and CS were almost identical, but the second stage had a significant difference. With regard to RM and CM, the most possible mechanisms for moisture release (zone 1) and chars oxidation (zone 5) were $(1–x)^{3/2}$ and $(1–x)^{3/4}$, respectively. On basis of Section 3.1, the thermal oxidative degradation process of oil–plant meals at the second stage could be subdivided into the combustion of hemicellulose, cellulose, and lignin, respectively. Since the combustion process of cellulose and lignin in RM was indistinguishable, it meant that these two zones had a same reaction mechanism. It could be seen that the combustion models for hemicellulose and lignin in RM and CM were identical, but the models for cellulose were different. Comparing the values of E between RM and CM, it was found that the values for the release of moisture and light volatiles were almost identical, but the values for other zones were quite distinct. It was closely related to the contents of chemical components in RM and CM. To validate the exactness of above kinetics analysis, the fit between experimental data and theoretical values was checked. Based on Eq. (5), the value of x can be calculated as a function of reaction temperature T through using the kinetic parameters in Table 4. As seen from Fig. 4, the calculated line and experimental data were almost similar, which indicated that the kinetic triplets can accurately predict and reproduce the thermal oxidative degradation process of RS, RM, CS, and CM.

Since

$$\Delta H = E - RT_p \quad (11)$$

where the value of E was predetermined by Coats–Redfern approach; The change of enthalpy (ΔH) is the state function of a chemical reaction that reflects heat absorbed or released under constant pressure (Li et al., 2015a, b); The change of Gibbs free energy (ΔG) for the activated complex formation from the reagents can be estimated by the thermodynamic equation (Xu and Chen, 2013; Li et al., 2015a).

$$\Delta G = \Delta H - T_p \Delta S \quad (12)$$

The thermodynamic parameters from the thermal oxidative degradation of oil–plant residues were very significant to provide information on the design, upgrading, and scaling of industrial combustors, as well as the optimization of operations. Table 5 illustrated the changes of enthalpy ΔH, Gibbs free energy ΔG, and entropy ΔS from the thermal oxidative decomposition of RS, RM, CS, and CM at T_p, of 10 K min^{-1}. The parameter of ΔH revealed the energy barrier between the activated complex and reagents. If the ΔH value is small, the formation of the activated complex is more favored. It was found that the values of ΔH at T_{p1}, T_{p3}, and T_{p5} for RS were greater than those for RM, meaning that the activated complex formed during the thermal oxidative degradation of RM was more favored. For CS and CM, the values of ΔH at T_{p1} and T_{p5} for CS were greater, but the ΔH value at T_{p3} was smaller.

The thermal oxidative decomposition of RS, RM, CS, and CM occurred at T_{p1} was mainly due to the release of moisture and light volatile components. With the oxidizing temperature increasing, the chemical bonds began to break. The parameter of ΔG reflects the increase in total energy of the system at the approach of the reagents and the formation of activated complex (Li et

4. Conclusions

TG-DTG-DSC experiments revealed that the thermal oxidative degradation of oil-plant residues could be distinguished as moisture evaporation, release and combustion of volatiles, and chars oxidation. The thermal characteristics were highly influenced by biomass species and heating rates as revealed by several combustion characteristic parameters. Kinetics analysis results indicated that the most appropriate mechanisms for various thermal zones were order reaction models. The calculated kinetic parameters could well simulate thermal data, and the kinetic compensation effect was evident. As for thermodynamic analysis, the variation trends of ΔH, ΔG, and ΔS at peak temperatures for RS (RM) were similar to CS (CM).

Acknowledgement

Grateful acknowledgement is made to associate Professor Lin Mu and Professor Hongchao Yin (Dalian University of Technology) whose constructive comments have helped to improve the quality of this paper. Financial support for this work that has been provided by the Fundamental Research Funds for the Central Universities (2017BQ062) is also gratefully acknowledged.

Appendix A. Supplementary data

Supplementary data associated with this article can be found, in the online version.

References

1. Açıkalın, K., 2012. Pyrolytic characteristics and kinetics of pistachio shell by thermogravimetric analysis. J. Therm. Anal. Calorim. 109, 227–235.

2. Bhattacharya, M., Paramati, S. R., Ozturk, I., Bhattacharya, S., 2016. The effect of renewable energy consumption on economic growth: Evidence from top 38 countries. Appl. Energy 162, 733–741.

3. Boonchom, B., Puttawong, S., 2010. Thermodynamics and kinetics of the dehydration reaction of $FePO_4 \cdot 2H_2O$. Physica B 405, 2350–2355.

4. Budrugeac, P., Segal, E., 2001. Some methodological problems concerning nonisothermal kinetic analysis of heterogeneous solid–gas reactions. Int. J. Chem. Kinet. 33, 564–573.

5. Chen, C., Ma, X., Liu, K., 2011. Thermogravimetric analysis of microalgae combustion under different oxygen supply concentrations. Appl. Energy 88, 3189–3196.

6. Chen, J., Fan, X., Jiang, B., Mu, L., Yao, P., Yin, H., Song, X., 2015a. Pyrolysis of oil–plant wastes in a TGA and a fixed–bed reactor: Thermochemical behaviors, kinetics, and products characterization. Bioresour. Technol. 192, 592–602.

7. Chen, J., Mu, L., Cai, J., Yao, P., Song, X., Yin, H., Li, A., 2015b. Pyrolysis and oxy–fuel combustion characteristics and kinetics of petrochemical wastewater sludge using thermogravimetric analysis. Bioresour. Technol. 198, 115–123.

8. Chen, Y., Duan, J., Luo, Y. H., 2008. Investigation of agricultural residues pyrolysis behavior under inert and oxidative conditions. J. Anal. Appl. Pyrolysis 83, 165–174.

9. Chen, Z., Hu, M., Zhu, X., Guo, D., Liu, S., Hu, Z., Xiao, B., Wang, J., Laghari, M., 2015c. Characteristics and kinetic study on pyrolysis of five lignocellulosic biomass via thermogravimetric analysis. Bioresour. Technol. 192, 441–450.

10. Du, Y., Jiang, X., Lv, G., Ma, X., Jin, Y., Wang, F., Chi, Y., Yan, J., 2014. Thermal behavior and kinetics of bio–ferment residue/coal blends during co–pyrolysis. Energy Convers. Manage.88, 459–463.

11. Du, Y., Jiang, X., Ma, X., Liu, X., Lv, G., Jin, Y., Wang, F., Chi, Y., Yan, J., 2013. Evaluation of cofiring bioferment residue with coal at different proportions: combustion characteristics and

kinetics. Energy Fuels 27, 6295–6303.

12. Fournel, S., Marcos, B., Godbout, S., Heitz, M., 2015. Predicting gaseous emissions from small–scale combustion of agricultural biomass fuels. Bioresour. Technol. 179, 165–172.

13. Gai, C., Liu, Z., Han, G., Peng, N., Fan, A., 2015. Combustion behavior and kinetics of low–lipid microalgae via thermogravimetric analysis. Bioresour. Technol. 181, 148–154.

14. Hassan, H., Lim, J. K., Hameed, B. H., 2016. Recent progress on biomass co–pyrolysis conversion into high–quality bio–oil. Bioresour. Technol. 221, 645–655.

15. Idris, S. S., Rahman, N. A., Ismail, K., 2012. Combustion characteristics of Malaysian oil palm biomass, sub–bituminous coal and their respective blends via thermogravimetric analysis (TGA). Bioresour. Technol. 123, 581–591.

16. Kravanja, Z., Varbanov, P. S., Klemeš, J. J., 2015. Recent advances in green energy and product productions, environmentally friendly, healthier and safer technologies and processes, CO_2. Clean Technol. Environ. Policy 17, 1119–1126.

17. Li, H., Niu, S., Lu, C., Wang, Y., 2015a. Comprehensive Investigation of the Thermal Degradation Characteristics of Biodiesel and Its Feedstock Oil through TGA–FTIR. Energy Fuels 29, 5145–5153.

18. Li, H., Niu, S. L., Lu, C. M., Cheng, S. Q., 2015b. Comparative evaluation of thermal degradation for biodiesels derived from various feedstocks through transesterification. Energy Convers. Manage. 98, 81–88.

19. Li, X.G., Lv, Y., Ma, B.G., Jian, S.W., Tan, H.B., 2011. Thermogravimetric investigation on co–combustion characteristics of tobacco residue and high–ash anthracite coal. Bioresour. Technol. 102, 9783–9787.

20. Liu, X., Chen, M., Yu, D., 2013. Oxygen enriched co–combustion characteristics of herbaceous biomass and bituminous coal. Thermochim. Acta 569, 17–24.

21. Meng, F., Yu, J., Tahmasebi, A., Han, Y., 2013. Pyrolysis and combustion behavior of coal gangue in O_2/CO_2 and O_2/N_2 mixtures using thermogravimetric analysis and a drop tube furnace. Energy Fuels 27, 2923–2932.

22. Mui, E. L., Cheung, W. H., Lee, V. K., McKay, G., 2010. Compensation effect during the pyrolysis of tyres and bamboo. Waste Manage. 30, 821–830.

23. Munir, S., Daood, S. S., Nimmo, W., Cunliffe, A. M., Gibbs, B. M. 2009. Thermal analysis and devolatilization kinetics of cotton stalk, sugar cane bagasse and shea meal under nitrogen and air atmospheres. Bioresour. Technol. 100, 1413–1418.

24. Ogle, S. M., Olander, L., Wollenberg, L., Rosenstock, T., Tubiello, F., Paustian, K., Buendia, L., Nihart, L., Smith, P., 2014. Reducing greenhouse gas emissions and adapting agricultural management for climate change in developing countries: providing the basis for action. Global Change Biol. 20, 1–6.

25. Omer, A. M., 2008. Energy, environment and sustainable development. Renewable Sustainable Energy Rev. 12, 2265–2300.

26. Quan, C., Gao, N., Song, Q., 2016. Pyrolysis of biomass components in a TGA and a fixed–bed reactor: Thermochemical behaviors, kinetics, and product characterization. J. Anal. Appl. Pyrolysis 121, 84–92.

27. Tahmasebi, A., Kassim, M. A., Yu, J., Bhattacharya, S., 2013. Thermogravimetric study of the combustion of *Tetraselmis suecica* microalgae and its blend with a Victorian brown coal in O_2/N_2 and O_2/CO_2 atmospheres. Bioresour. Technol. 150, 15–27.

28. Vlaev, L., Nedelchev, N., Gyurova, K., Zagorcheva, M., 2008. A comparative study of non–isothermal kinetics of decomposition of calcium oxalate monohydrate. J. Anal. Appl. Pyrolysis 81, 253–262.

29. Vyazovkin, S., Burnham, A.K., Criado, J.M., Pérez–Maqueda, L.A., Popescu, C., Sbirrazzuoli, N., 2011. ICTAC Kinetics Committee recommendations for performing kinetic computations on thermal analysis data. Thermochim. Acta 520, 1–19.

30. Werther, J., Saenger, M., Hartge, E. U., Ogada, T., Siagi, Z., 2000. Combustion of agricultural residues. Prog. Energy Combust. Sci. 26, 1–27.

31. Wu, K., Liu, J., Wu, Y., Chen, Y., Li, Q., Xiao, X., Yang, M., 2014. Pyrolysis characteristics and kinetics of aquatic biomass using thermogravimetric analyzer. Bioresour. Technol. 163, 18-25.

32. Xu, Y., Chen, B., 2013. Investigation of thermodynamic parameters in the pyrolysis conversion of biomass and manure to biochars using thermogravimetric analysis. Bioresour. Technol. 146, 485–493.

33. Yahya, M. A., Al–Qodah, Z., Ngah, C. Z. 2015. Agricultural bio–waste materials as potential sustainable precursors used for activated carbon production: a review. Renewable Sustainable Energy Rev. 46, 218–235.

34. Zhou, C., Liu, G., Cheng, S., Fang, T., Lam, P. K. S., 2014. Thermochemical and trace element behavior of coal gangue, agricultural biomass and their blends during co–combustion. Bioresour. Technol. 166, 243–251.

35. Zhou, X., Wang, F., Hu, H., Yang, L., Guo, P., Xiao, B., 2011. Assessment of sustainable biomass resource for energy use in China. Biomass Bioenergy 35, 1–11.

36. Zhu, X., Chen, Z., Xiao, B., Hu, Z., Hu, M., Liu, C., Zhang, Q., 2015. Co–pyrolysis behaviors

ACCEPTE

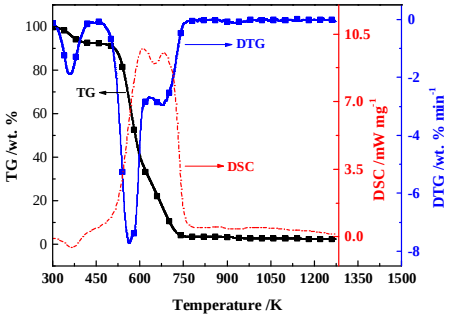

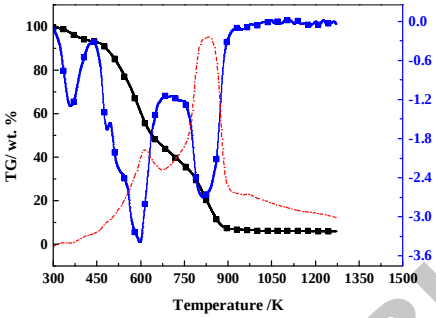

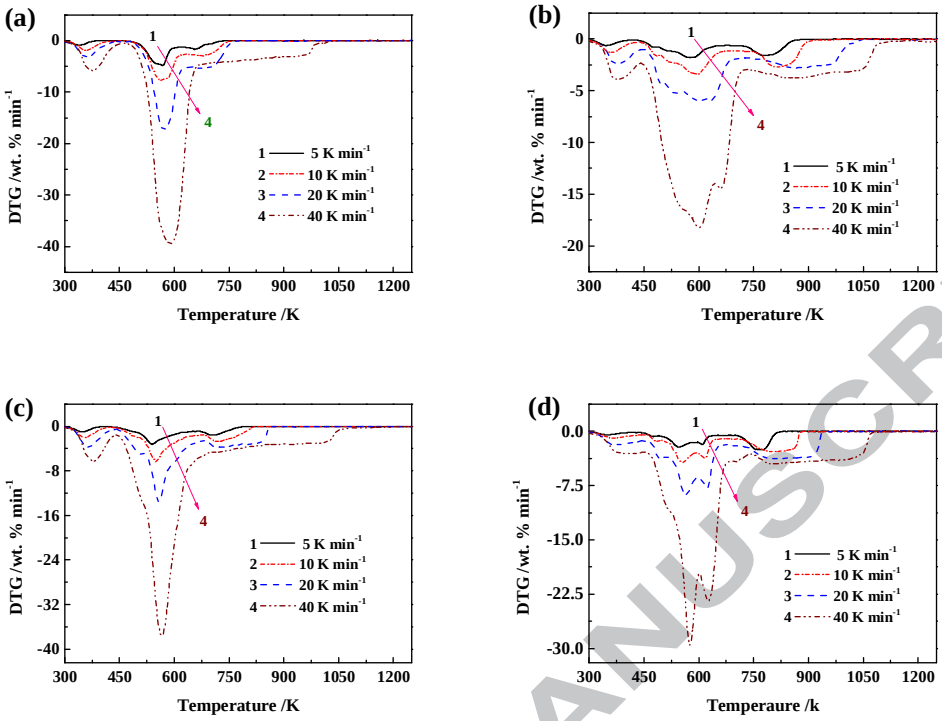

Fig. 3. DTG curves for thermal oxidative decomposition of (a) RS, (b) RM, (c) CS, and (d) CM at 5, 10, 20, and 40 K min^{-1}

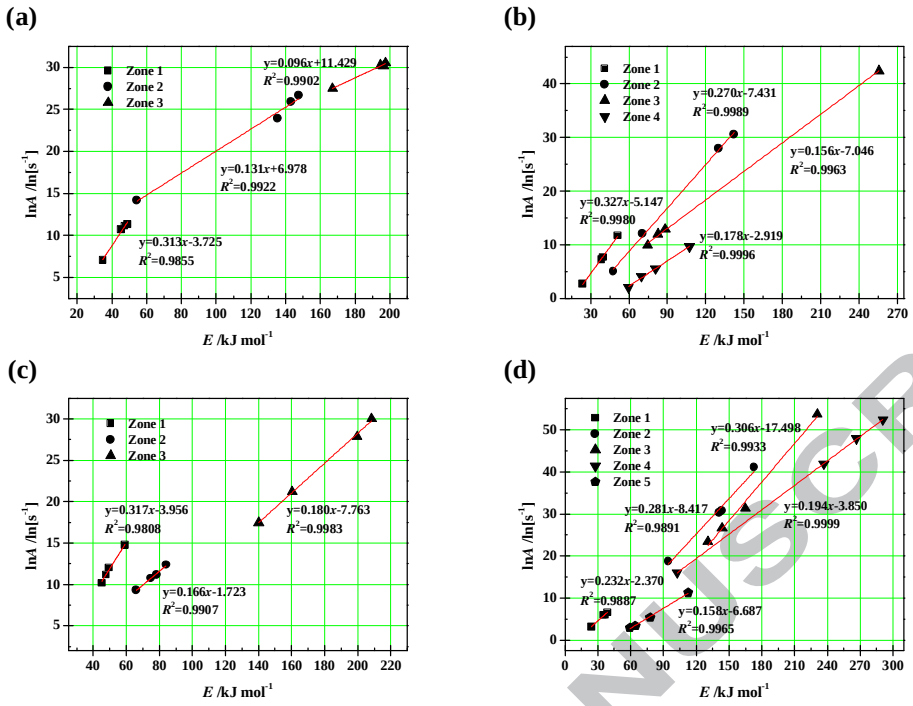

Fig. 5. Kinetic compensation effect analysis for thermal oxidative decomposition of (a) RS, (b) RM, (c) CS, and (d) CM at different heating rates

List captions of Tables:

Table 1 Proximate analysis and ultimate analysis for four typical oil–plant residues

Table 2 Thermal oxidative decomposition characteristic parameters of oil–plant residues at 10 K min^{-1}

Table 3 Thermal oxidative decomposition characteristic parameters of RS at 5, 10, 20, and 40 K min^{-1}

Table 4 Kinetic parameters of the thermal oxidative decomposition of RS, RM, CS, and CM at 10 K min^{-1}

Table 5 Thermodynamic parameters of the thermal oxidative decomposition of RS, RM, CS, and CM at 10 K min^{-1}

Table 1

Ultimate analysis and proximate analysis for four typical oil–plant residues

Samples	Rape straw	Rapeseed meal	Camellia seed shell	Camellia seed meal
Pictures				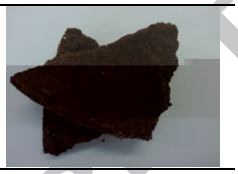
Proximate analysis (wt. %, ar[c])				
Moisture (M)	6.32	4.07	4.94	4.38
Volatile matter (VM)	71.55	77.33	69.71	74.05
Fixed carbon (FC)	17.05	11.62	21.10	18.96
Ash (A)	5.08	6.98	4.25	2.61
Ultimate analysis (wt. %, daf[a])				
Carbon (C)	44.39	48.62	46.05	50.64
Hydrogen (H)	6.47	7.45	6.08	7.12
Nitrogen (N)	0.54	5.50	0.37	1.16
Sulfur (S)	0.36	0.97	0.17	0.31
Oxygen (O)[b]	48.24	37.46	47.33	40.77

[a] Dry ash free basis.

[b] Calculated by difference.

[c] As received basis.

Table 2

Thermal oxidative decomposition characteristic parameters of oil–plant residues at 10 K min^{-1}

Samples	T_i[a]	T_p[b]				$-R_p$[c]				$-R_v$[d]	T_b[e]	$10^7 \times D_v$[f]	$10^3 \times C_i$[g]	$10^4 \times C_b$[h]	$10^8 \times S$[i]
		T_{p2}	T_{p3}	T_{p4}	T_{p5}	$-R_{p2}$	$-R_{p3}$	$-R_{p4}$	$-R_{p5}$						
RS	512.3		562.1		675.3		7.73		2.97	3.46	756.5	4.52	12.93	10.09	13.47
RM	493.2	484.4	596.2		810.2	1.69	3.41		2.71	1.83	932.2	1.49	5.53	2.05	2.75
CS	492.2		549.5		715.3		6.33		2.70	2.54	814.7	4.60	12.22	8.55	8.15
CM	518.3	483.9	554.5	616.5	797.9	1.41	4.28	3.72	2.85	2.29	877.7	2.98	7.16	4.91	4.16

[a] T_i, the ignition temperature, K.

[b] T_p, the peak temperature of each zone, K; T_{p1}, T_{p2}, T_{p3}, T_{p4}, and T_{p5} are the peak temperature of the first, second, third, fourth, and fifth peak, respectively.

[c] $-R_p$, the maximum weight loss rate of each zone, wt. % min^{-1}; $-R_{p1}$, $-R_{p2}$, $-R_{p3}$, $-R_{p4}$,and $-R_{p5}$ are the value of the first, second, third, fourth, and fifth peak, respectively.

[d] $-R_v$, the average weight loss rate, wt. % min^{-1}.

[e] T_b, the burnout temperature, K.

[f] D_v, the volatile matter release index, wt. % min^{-1} K^{-3}.

[g] C_i, the ignition index, wt. % min^{-3}.

[h] C_f, the burnout index, wt. % min^{-4}.

[i] S, the comprehensive combustibility index, wt. $\%^2$ min^{-2} K^{-3}.

Table 3

Thermal oxidative decomposition characteristic parameters of RS at 5, 10, 20, and 40 K min^{-1}

β^a	T_i	T_p			$-R_p$				$-R_v$	T_b	$10^7 \times D_v$	$10^3 \times C_i$	$10^3 \times C_b$	$10^7 \times S$
		T_{p1}	T_{p3}	T_{p4}	T_{p5}	$-R_{p1}$	$-R_{p3}$	$-R_{p4}$	$-R_{p5}$						
5	508.5		567.9		655.7		4.83		1.71	1.86	736.9	2.01	1.99	0.06	0.47
10	512.3		562.1		675.3		7.73		2.97	3.46	756.5	4.52	12.93	1.01	1.35
20	516.5		570.7		672.7		17.27		5.42	6.81	767.7	10.40	109.6	18.57	5.74
40	522.3		589.1		724.3		39.50		4.22	7.32	1033.9	14.29	721.1	186.7	10.25

[a] β, heating rate, K min^{-1}.

Table 4

Thermodynamic parameters of the thermal oxidative decomposition of RS, RM, CS, and CM at 10 K min^{-1}

Parameters	Units	RS	RM	CS	CM
T_{p1}	K	358.50	355.40	355.90	366.50
ΔH_1	kJ mol^{-1}	46.07	35.46	42.22	33.44
ΔG_1	kJ mol^{-1}	103.65	104.49	102.77	108.69
ΔS_1	J mol^{-1} K^{-1}	–160.61	–194.24	–170.14	–205.30
T_{p2}	K		484.40		483.90
ΔH_2	kJ mol^{-1}		126.07		136.80
ΔG_2	kJ mol^{-1}		138.19		139.05
ΔS_2	J mol^{-1} K^{-1}		–25.03		–4.66
T_{p3}	K	562.10	596.20	549.50	554.50
ΔH_3	kJ mol^{-1}	130.79	69.66	67.16	126.08
ΔG_3	kJ mol^{-1}	164.21	175.05	160.05	161.36
ΔS_3	J mol^{-1} K^{-1}	–59.46	–176.76	–169.05	–63.62
T_{p4}	K				616.50
ΔH_4	kJ mol^{-1}				285.68
ΔG_4	kJ mol^{-1}				176.68
ΔS_4	J mol^{-1} K^{-1}				176.81
T_{p5}	K	675.30	810.20	715.30	797.90
ΔH_5	kJ mol^{-1}	190.81	100.59	193.69	71.17
ΔG_5	kJ mol^{-1}	197.21	247.29	214.29	244.17
ΔS_5	J mol^{-1} K^{-1}	–9.48	–181.06	–28.79	–216.82

Highlights:

- Thermal oxidative degradation of four oil–plant residues was studied by TG–DTG–DSC
- Thermal behaviors of oil–plant residues were affected by species and heating rates
- Kinetics was analyzed by CR approach, and the kinetic compensation effect was evident
- Thermodynamic parameters (ΔH, ΔG, ΔS) were obtained by the activated complex theory.